Available online at www.sciencedirect.com
ScienceDirect
Journal of Nuclear Materials 363–365 (2007) 1129–1137
journal of nuclear materials
www.elsevier.com/locate/jnucmat

Binary beryllium–tungsten mixed materials

Ch. Linsmeier [a,*], K. Ertl [a], J. Roth [a], A. Wiltner [a], K. Schmid [a], F. Kost [a], S.R. Bhattacharyya [a,1], M. Baldwin [b], R.P. Doerner [b]

[a] Max-Planck-Institut für Plasmaphysik, EURATOM Association, Boltzmannstr. 2, 85748 Garching b. München, Germany
[b] Center for Energy Research, University of California – San Diego, MC 0417, 9500 Gilman Dr., La Jolla, CA 92093-0417, USA

Abstract

Both Be and W are planned as wall materials for ITER. Although these materials will dominate the ITER first wall, and despite the fact that their interaction during operation will be dominated by surface processes, mostly bulk material data on the Be–W binary system are available. This article describes investigations of thin films of Be deposited on W, the inverse system (W films on Be), as well as experiments where W surfaces are exposed to a Be-seeded deuterium plasma. The formed alloy phases Be_2W and $Be_{12}W$ are identified by X-ray photoelectron spectroscopy (XPS) and depth profile data both from sputter-XPS and MeV ion beam analysis are presented.

PACS: 68.55.Nq; 79.60.Dp; 79.60.Jv; 82.80.Pv

Keywords: Beryllium; Diffusion; First wall; Surface analysis; Tungsten

1. Introduction

The planned application of both metals beryllium and tungsten together as first wall materials of the next step fusion device ITER is based on the foreseen advantageous properties of these metals for the respective locations in the plasma vessel [1]. Erosion, transport, and redeposition of both materials during operation will lead to transport of elements onto surfaces of different materials. Due to kinetic energy of impinging particles and elevated wall temperatures, alloys and compounds consisting of the present elements will be formed. These 'mixed materials' exhibit strongly altered physical and chemical properties compared to the intended properties of the pure elements which were originally installed. Of all binary systems considered in previous studies, beryllium–tungsten received least attention although Be–W alloys bear the potential of drastically reduced melting temperatures compared to pure W. For the formation of a binary Be–W alloy, two possible scenarios can be envisaged in a fusion device: deposition of tungsten on beryllium surface or vice versa. In this paper we investigate both Be films deposited on W substrates and the reverse system (W films on Be substrates), as well as the interaction of a Be-seeded deuterium plasma with W substrates. The interaction of the depositing

* Corresponding author. Tel.: +49 89 32992285; fax: +49 89 3299962285.
E-mail address: linsmeier@ipp.mpg.de (Ch. Linsmeier).
[1] Permanent address: Surface Physics Division, Saha Institute of Nuclear Physics, 1/AF Bidhan Nagar, Kolkata 700 064, India.

0022-3115/$ - see front matter © 2007 Elsevier B.V. All rights reserved.
doi:10.1016/j.jnucmat.2007.01.224

species with the substrate is determined by the kinetic energy of the incoming particle and by the substrate temperature. Therefore, in the experiments with thin surface layers (Be/W and W/Be), thermal treatments are carried out in vacuum. Subsequently, the surface is investigated by ion beam accelerator-based techniques (Rutherford backscattering spectroscopy, RBS, and nuclear reaction analysis, NRA) and X-ray photoelectron spectroscopy (XPS). By XPS analysis, additional chemical information on the formed Be phases is gained. The W layers which were exposed to Be-seeded D plasmas are also analyzed in their chemical and elemental composition by NRA and XPS. The observations are discussed in order to assess the risks and consequences of the Be–W alloy formation in a fusion device which employs both metals as first wall materials.

This paper reviews the current knowledge on surface reactions in the Be–W system. A bulk phase diagram is available in the literature [2].

2. Experiments

The interaction of beryllium and tungsten is investigated in two different layered systems where both tungsten and beryllium are used as surface layer, respectively (W/Be: tungsten layer on beryllium; Be/W: beryllium layer on tungsten). The first series of experiments uses mechanically and electrochemically polished Be metal substrates (polycrystalline). Tungsten is deposited in a magnetron sputter device (base pressure: 2×10^{-5} Pa) with a layer thickness of 200 nm. Before starting the Be deposition, the surface is etched in a pure Ar plasma. The Be films on polycrystalline tungsten are deposited in a UHV chamber connected directly to the XPS analysis chamber to avoid air transfer of the reactive Be films. The base pressure in the preparation chamber is below 2×10^{-8} Pa, during the Be deposition the pressure is below 4×10^{-8} Pa. The substrates are cleaned using alternating sputter (3 kV, Ar^+) annealing (up to 970 K) cycles until no impurities are detected in XPS survey scans. During deposition of the surface layers, the substrates are kept at room temperature (300 K). The alloying of the two components is studied by annealing the samples to different temperatures in the XPS analysis chamber (base pressure better than 2×10^{-8}), whereby the pressure rises up to 5×10^{-8}. The samples are analyzed after annealing steps by XPS and RBS. XPS is performed in situ for the Be/W experiments. In case of the W/Be samples, for the RBS analysis air transfers were unavoidable.

XPS analysis is carried out in a PHI ESCA 5600 spectrometer using the monochromatic X-ray source (Al Kα, 1486.6 eV). The best spectral resolution in this mode is 0.26 eV. The analyzed area is 0.8 mm in diameter. XPS measurements are performed under a take-off angle of 22° with respect to the surface normal, depth profiles at 45°. The binding energy (BE) scale is referred to the Au $4f_{7/2}$ signal at 84.0 eV and calibrate additionally with the Cu $2p_{3/2}$ and Ag $3d_{5/2}$ signals [3]. High resolution spectra (pass energy 2.95 eV) are used to determine chemical binding states, in particular the chemical shift due to alloying. For quantitative measurements, survey scans with a pass energy of 93.90 eV are used. Chemical data analysis is carried out by fitting Gauss–Lorentz functions to the data, taking into account the background in the Be 1s region by a Shirley background [4]. Ion beam analysis was carried out at the Garching 3 MV tandem accelerator. Standard ion beam analysis techniques (RBS with ^{1}H, ^{3}He, and ^{4}He, scattering angle 165°) were applied. Reliable depth profiles from the RBS spectra are obtained using 'backward' and 'forward' calculations in combination, the 'IBA Data Furnace NDF' program [5] for solving the inverse RBS problem and the 'SIMNRA' program [6] for simulation of the spectra. In these calculations advantage is taken from the fact that for each experimental condition spectra measured with two different ion species and energies are available which entered the fit procedures simultaneously. As a constraint the total amount of W was kept constant. Cross sections for the ^{9}Be(p,α)^{6}Li and the ^{9}Be(p,d)^{8}Be reactions are extrapolated for the scattering angle of 165° from 138° data by Thomas et al. [7].

3. Results and discussion

3.1. Tungsten films on beryllium (W/Be)

The 200 nm W layer on beryllium which is discussed here is prepared and analyzed as described in Section 2, with an unavoidable air transport between annealing and RBS analysis steps. The final sputter XPS depth profile comprises both survey spectra for quantitative analysis and high-resolution spectra to determine the chemical binding states.

The changes of the W layer during the annealing sequence can be followed in the RBS spectra with

^{1}H and ^{4}He, respectively. Using protons has the advantage to make changes in the Be profile visible. The cross section for protons scattered from beryllium is non-Rutherford for the applied energies and yields an enhanced signal for Be. Fig. 1(a) shows the series of RBS spectra measured with protons at 1 MeV primary energy. The spectra are plotted on a semi-logarithmic scale to demonstrate the changes both in the Be and the W signals. Clearly two temperature regimes can be distinguished. Below 1000 K, only very small changes in the spectra are visible. The signal corresponding to the W layer (the W surface edge is located at channel 276) shows only small changes, both in position and intensity. The shift of about 1 channel between 300 K and 970 K is not above experimental uncertainties. At 1070 K, however, shifting of the W edge continues and supports the trend visible at lower temperatures. This shift indicates that tungsten is not any more present at the surface of the sample, but is continually replaced by another surface layer. The solution which element is present at the surface can be found in the Be signal. The Be edge is located at channel 166 in the spectra measured between 300 K and the run at 970 K. No significant difference is visible between these spectra. The Be edge after the first run at 1070 K is still at channel 166, but already intensity appears at channel 181. The Be surface edge is located at this position, therefore Be must be present at the sample surface after the first 1070 K annealing step. During the extended annealing at 1070 K, the Be edge continuously shifts from the 300 K position to the surface edge. The Be surface peak is still visible for annealing times up to 300 min (fine blue lines in Fig. 1(a)). After 360 min annealing, the Be edge lost the surface peak and exhibits the continuous characteristics for a smooth Be depth distribution.

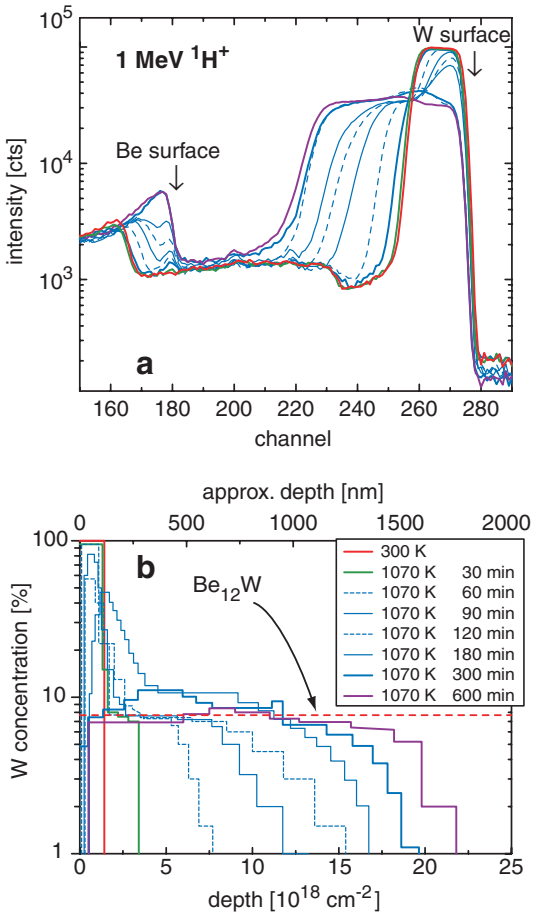

Fig. 1. RBS spectra (a) and depth profiles (b) measured with 1 MeV ^{1}H at a scattering angle of $\theta = 165°$, after annealing of a 200 nm W film on Be to the indicated temperatures/times.

The evolution of a smooth depth distribution is also observed in the tungsten signal. As discussed above, no significant deviations from the 300 K signal are observed up to 970 K. At 1070 K, the W surface signal changes. After 30 min, the leading edge still is at the surface position (within the experimental accuracy), but the trailing edge shifts by three channels to greater depths. This indicates the begin of the interdiffusion of Be and W at the layer-substrate interface. With continued annealing at 1070 K, the intermixing proceeds and also a decrease of the maximum W intensity is observed. During the time evolution and proceeding intermixing, however, the W from the surface layer is not lost into the Be bulk by diffusion. After the maximum time at 1070 K (600 min), there still exists a steep W trailing edge. This indicates that a well-defined intermixed W–Be layer has been formed. A diffusive loss of W into the Be bulk can therefore be excluded. During the annealing, also the leading edge of the W signal shifts to a final position in channel 274.

The observations from the ^{1}H RBS spectra are corroborated in the ^{4}He RBS spectra (not shown). From both series the depth profiles after the respective annealing steps can be calculated, shown in Fig. 1(b). In the semi-logarithmic diagram the tungsten concentration profile is plotted against the particle areal density. This areal density is converted into an approximate depth scale (given in the upper axis) by using the beryllium bulk density (1.85 g cm^{-3}, therefore 10^{15} Be per cm^{2} correspond

to 8.09×10^{-11} m). The initially rectangular W profile of the deposited tungsten layer continually broadens during the annealing steps at 1070 K. The dashed line corresponds to the $Be_{12}W$ composition. During the continued intermixing between tungsten and beryllium, the composition converges to $Be_{12}W$. Deviations from this composition are only observed at the intermixing front. However, the majority of the intermixed layer keeps this composition. After 600 min at 1070 K the profile is almost rectangular. In particular, the W concentration gradient is not exponentially extending into greatest depths, but has a fairly well-defined cut-off. This depth distribution leads to the conclusion that the formed $Be_{12}W$ layer has high stability and is not the result of a dissolution process of tungsten into the Be bulk.

From the front of the $Be_{12}W$ depth distribution a diffusion coefficient D can be estimated. Assuming a two-dimensional diffusion of the W layer into the Be bulk driven by the concentration gradient, the diffusion length x is defined by: $x = \sqrt{4Dt}$. This definition is derived from Fick's two laws and considers net diffusion towards the region of lower concentration due to random-walk motion. Since it neglects any driving forces due to gradients in the chemical potential, this value is only an estimation of D. Fitting the depth of the diffusion front with the above equation results in a diffusion coefficient D of 1.6×10^{-13} cm^2 s^{-1}. The fitted function reproduces well the data points. Therefore, the assumption of a diffusive intermixing is justified.

The question of the formed phase is addressed in XPS measurements at different depths. These depths are accessed by sputter profiling with 3 keV Ar^+. Between the sputtering cycles, XPS spectra in survey resolution are measured to detect impurities and perform elemental quantification. High-resolution spectra of the Be 1s region allow the identification of chemical binding states. The survey spectra demonstrate the purity of the deposited layers. Only signals from the elements W, Be, O, and C are detected, besides Ar from the sputtering process. The depth profiles for the elements Be, W, C, and O are plotted in Fig. 2. The logarithmic fluence scale makes the changes in the surface-near region visible together with the composition in greater depths. Please note that the intermixed layer dominates the total depth under investigation: This layer extends from Ar^+ fluences of 3.5×10^{17} cm^{-2} to 7.5×10^{18} cm^{-2}, corresponding to an estimated depth of 3 μm. The average composition in this

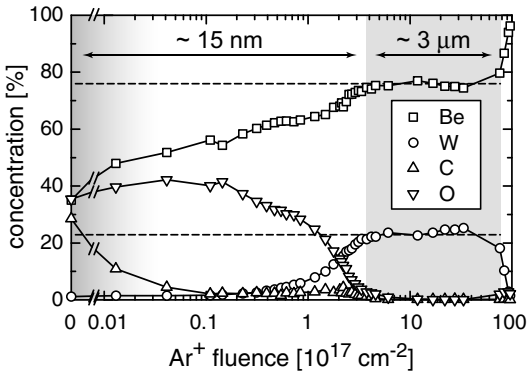

Fig. 2. Depth profile of the formed Be–W layer on a Be substrate after annealing at 1070 K for 600 min. The composition of the intermixed layer is practically constant between Ar^+ fluences of 3.5×10^{17} cm^{-2} and 7.5×10^{18} cm^{-2}.

depth interval from the XPS analysis is 75.7% W and 22.9% Be. This nominal stoichiometry of $Be_{3.3}W$, however, is not the true stoichiometry of the intermixed layer, as determined in the RBS analysis. Since Ar^+ bombardment leads to a strong preferential sputtering (see e.g. [10]), the composition determined here deviates from the true stoichiometry. To compare the XPS results with the RBS data, we calculate the partial sputtering yields of a $Be_{12}W$ alloy for the present Ar^+ bombardment conditions using the Monte Carlo code SDTRIM.SP [11]. Taking into account the resulting yields of $Y_W = 0.21$ and $Y_{Be} = 3.34$, the calculated stoichiometry is Be_9W, close to the stoichiometry $Be_{12}W$, determined by ion beam analysis. Therefore it can be concluded that the deviation of the XPS composition from the IBA compositions is caused mostly by preferential sputtering effects. In contrast to the intermixed $Be_{12}W$ zone, the surface layer does not contain tungsten: the tungsten concentration at small fluences is in the 1–3% range. However, this surface zone (detected up to an Ar^+ fluence of approximately 1×10^{17} cm^{-2}, corresponding to a depth of ≈15 nm) contains oxygen in reasonable amounts. From the XPS quantitative data, a surface layer of BeO can be concluded. Carbon is only present at the very surface of the sample and is easily removed by sputtering with a fluence of 4×10^{15} cm^{-2}. This is the typical signal from an adsorbed contamination layer caused by sample transport through the air. These results corroborate the interpretation of the RBS data where small shifts in the tungsten surface edge were observed (see Fig. 1(a)). Indeed, the Ar^+ depth profile proves the existence of a Be-containing surface layer. Since

oxygen is of no importance at greater depths of the sample, this element must be introduced during the annealing/measurement steps. As shown in the legends in the Figures of the RBS spectra and the IBA depth profile (Fig. 1), several annealing and analysis cycles were carried out. The XPS depth profile is measured after the final annealing step at 1070 K. As discussed above, the W edge shifts to lower channels during the annealing at 1070 K. Therefore, at this temperature a Be surface layer is formed. Initially, this layer must be metallic, since no oxygen reservoir is present in the sample. After air transfer, however, Be reacts with the air to BeO, finally forming the layer observed in Fig. 2. It remains an open question here whether this Be accumulation at the surface is a result of the adsorbed air (oxygen, water) at the surface and the oxide formation with these species as driving force, or whether the Be surface accumulation would also take place without oxide-forming species.

The depth profile is continued until the W signal is only small compared to the Be signal. Even without taking into account any preferential sputtering, it can be concluded that at this fluence the deposited tungsten is almost completely removed. The slight increase in the oxygen concentration at the interface between surface layer (tungsten at deposition time) and bulk (beryllium) can be attributed to a BeO layer at the original Be sample surface. Although a cleaning step in the magnetron device is applied before W deposition (sputtering by pure Ar plasma for 60 s), no evidence is available that the natural oxide layer at the Be surface is removed completely.

The analysis of the sample surface after each sputtering step during the depth profile with high-resolution spectra enables the assignment of chemical states to the Be signals. The Be 1s photoelectron region is deconvoluted using MultiPak [4]. Three Gauss–Lorentz functions are fitted to the data in the Be 1s region. In particular within the binding energy region where both the metallic and alloy signals appear, it is necessary to restrict the fit. Therefore, a fixed difference between the oxidic and metallic Be 1s peak positions of 3.0 eV is used. For the third component in the Be 1s signal all parameters are kept free. In Fig. 3 the composition of the Be 1s signal with respect to the chemical bond state of beryllium is shown. In the near-surface region, the oxidic species dominate. This is expected from the elemental composition shown in Fig. 2 where oxygen is detected in the near-surface region.

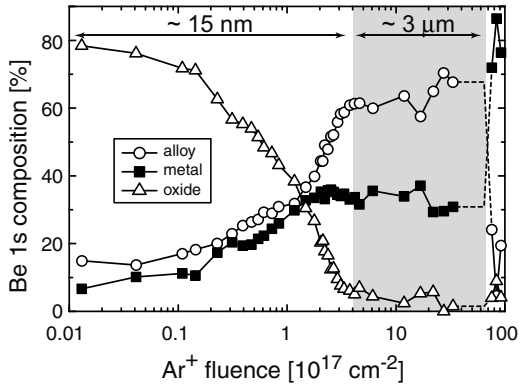

Fig. 3. Composition of the XPS Be 1s signal during the Ar^+ depth profiling. The hatched area between Ar^+ fluences of $4\times10^{17}\,cm^{-2}$ and $7.5\times10^{18}\,cm^{-2}$ represents the alloy zone. At the end of this zone, the trends are extrapolated (dashed lines), since at this fluence no high-resolution spectrum is available.

In this zone also only a few percent tungsten are present. The small oxygen fraction within the hatched alloy zone and also the at the end of the depth profile above $7.5\times10^{18}\,cm^{-2}$ shows a large scatter due to the small intensity in this region. The Be 1s intensity between approximately 113 and 118 eV is fitted by two peaks, labelled 'metallic' and 'alloy'. The resulting intensities and the difference in binding energy between these two peaks are plotted in Fig. 3. Up to a fluence of $2\times10^{17}\,cm^{-2}$, the metallic and alloy peak are approximately of the same intensity, with a slightly larger value for the alloy. At this fluence, the alloy peak gains intensity and reaches more than twice the strength in the shaded area where the $Be_{12}W$ is identified. At the interface to the Be bulk a sharp drop of alloy intensity is observed and finally the Be 1s signal is dominated by the metallic peak. The binding energy difference between metallic and alloy peak is practically constant in the alloy region and is 0.51 eV. Since the stoichiometry of this alloy layer is known from the RBS results, the BE of the Be 1s peak in the $Be_{12}W$ alloy is determined to 111.3 eV.

3.2. Beryllium films on tungsten (Be/W)

In this section, the interaction of thin Be films on a tungsten substrate, the inverse system compared to the W/Be films described in Section 3.1, are discussed. This situation is envisaged for Be being deposited on a W surface.

The Be films are deposited on polycrystalline tungsten at 300 K in a UHV preparation chamber

which is connected to an XPS analysis chamber, as described in Section 2. Sample preparation and analysis are carried out without transfer through the air. Despite the well-controlled vacuum conditions (see above) the deposited metal films are contaminated by oxygen with a maximum concentration of approximately 10% due to the high reactivity of Be. A detailed analysis is published in [8,9].

The deposited beryllium reacts already with the tungsten substrate at 300 K. Both in the Be 1s and W 4f signals a new component at lower BEs is necessary to fit the experimental data. The results for a 1.9 nm Be layer are shown in Fig. 4(a). The Be signal shows a peak at 114.8 eV for BeO and a large signal at lower BEs. This peak can only be fitted if two Gauss–Lorentz functions are used. During the fit procedure, the BE difference between the oxidic and metallic signal is kept constant at 3.0 eV. The additional Be 1s peak is located at 111.1 eV. This peak position results also from fits to Be layers with thicknesses from 0.5 nm to 4.8 nm. Below four monolayers a small variation in peak position towards

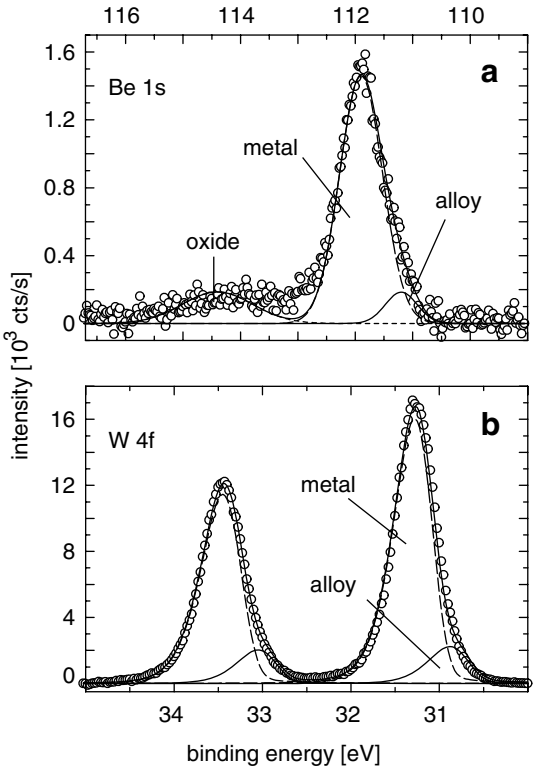

Fig. 4. Be 1s and W 4f signals measured at a 1.9 nm thick Be film on polycrystalline tungsten, deposited in UHV at 300 K. Both Be and W signals afford signals at lower BEs to fit the experimental data.

smaller BEs is observed. However, since the Be signal is very weak due to the small photoelectron cross section, thin Be layers of a few monolayers have a bad signal-to-noise ratio and therefore a larger uncertainty in the fitting results. The corresponding W 4f signals are shown in Fig. 4(b). Here, no oxidic peak is observed, although the W $4f_{7/2}$ signal shows a small broadening after Be deposition (from 0.45 to 0.50 eV). The formation of a W–O surface oxide, however, would lead to a broadening of this peak by 0.11 eV. The W 4f signals are fitted by asymmetric Gauss–Lorentz functions. During the fit procedure, the W $5p_{3/2}$ signal is taken as a reference at 37.0 eV. In addition, the peak positions of the W $4f_{7/2}$ and $4f_{3/2}$ peaks are fixed at the positions from literature [12] and measurements at the clean tungsten surface ($4f_{7/2}$ at 31.4, splitting 2.17 eV). Further, the peak area ratio due to the spin-orbit splitting is kept constant at 0.77 (determined also at the clean W surface, theory would require 0.75). These restraints to the fit procedure result in an additional W 4f doublet located at 31.0 eV (W $4f_{7/2}$). Other than the Be 1s signals, the W 4f peaks remain constant in BE for deposited layers with thicknesses between 0.5 and 4.8 nm, especially for Be layers in the monolayer range. From experiments with increasing deposited Be amounts it becomes evident that only the Be directly at the layer–substrate interface shows the additional peak in the Be 1s spectrum. At 300 K, all additional Be increases the metallic signal only.

The situation changes at elevated temperatures. The metallic Be is deposited at 300 K. Two different annealing procedures are compared for Be layers between 1.2 nm and 3.3 nm initial thicknesses. In the first procedure Be layers are annealed for 30 min to increasing temperatures up to 1070 K. After each annealing step, the Be intensity is determined and a remaining thickness is calculated. For the Be layer thickness calculation, both the substrate and the layer signals are used [13]. In addition, the Be 1s region in high-resolution spectra allows the observation of a proceeding reaction between Be and W. In the second series Be layers in the same thickness regime are annealed at constant temperatures for up to 30 h. The composition and layer thickness are measured at the respective elevated temperature. In all cases, the Be intensity decreases above an annealing temperature of 570 K. The decrease in Be intensity goes parallel with a decrease in Be layer thickness. Depending on the initial thickness, the final Be layer amounts

to 1.1–1.4 nm after 1070 K. In all cases examined here, no complete loss of Be in the surface zone accessible by XPS is observed. In case of the long-term annealing experiments, the decrease in Be thickness takes place already during the ramp-up to the respective annealing temperature. During the remaining time, no significant further decrease is observed. A sputter depth profile (using Ar^+ at 3 keV) of an untreated and an annealed Be layer demonstrates that the Be loss cannot be explained by a diffusion of Be into the W bulk [9]. The Be intensity drops to zero after a sputtering fluence of 6×10^{15} cm^{-2} applied to a remaining Be-containing layer of 1.2 nm. The only solution to explain the loss of Be from the surface is sublimation. The remaining Be at the surface starts to react with W at the same temperature at which the layer thickness decreases.

In Fig. 5 the spectra of three Be layers are plotted before and after annealing to 770, 870, and 970 K. The initial Be layers were 1.3, 1.5, and 2.1 nm, respectively. After annealing, all three layers have a thickness between 1.0 and 1.2 nm. These thicknesses are reached already after the comparatively short temperature ramp-up. Therefore, the excess Be is lost very quickly in the initial annealing phase. The spectra shown compare the initial status after room temperature deposition (marked r.t.) with the final state after the annealing to the indicated temperatures. Already after 770 K annealing not only a reduction in Be layer thickness, but also the onset of the alloying reaction is visible. Both W and Be signals shift to lower BEs. At 970 K the formation of a Be–W alloy leads even in the W 4f signal to a second peak which is already visible by

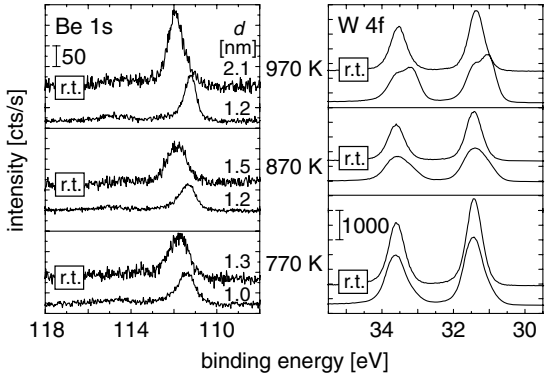

Fig. 5. Changes in the Be 1s and W 4f regions before and after long-term annealing to three different temperatures.

eye. Peak fitting to all signals yields Be:W ratios for the three temperatures of 5:1 (770 K), 3:1 (870 K), and 2:1 (970 K). This stoichiometry was also reached in the short-term annealing sequences discussed above. The final stoichiometry Be_2W is reached in the annealing of Be layers on W, but quantitatively only after annealing to at least 970 K. For this stoichiometry, the binding energies for Be 1s and W $4f_{7/2}$ are determined to 111.1 eV and 31.0 eV, respectively. The corresponding peak shifts with respect to the metal are 0.7 eV (Be 1s) and 0.4 eV (W 4f).

3.3. Interaction of Be-seeded deuterium plasmas with tungsten

In the PISCES-B device Be-seeded deuterium plasmas with variable Be fractions (0.001–0.01) can be produced [14] which are comparable in flux to the target surface to the expected fluxes for the ITER divertor (approximately 10^{19} cm^{-2} s^{-1}) [15]. During exposure, the target can be held at elevated temperatures under controlled conditions. Here we show the results of a tungsten sample which was exposed to a deuterium plasma at a sample temperature of 1260 K. The total flux at the sample was 8.0×10^{21} cm^{-2} s^{-1}. The Be concentration in the plasma was 0.4%, corresponding to a Be flux to the sample of 3.2×10^{19} cm^{-2} s^{-1}. The ion beam analysis of the sample by nuclear reaction analysis with 1 MeV ^{3}He yields a total amount of beryllium in the surface-near region accessible by NRA of 1.4×10^{17} cm^{-2}. No deuterium is measured in this sample due to the high exposition temperature. In the XPS survey spectra the elements W, Be, O, C, and La are detected. Lanthanum is present throughout the whole analyzed depth of $\approx$1.3 μm. Because of the large photoionization cross section, the La signals are quite prominent in the spectra. However, the total concentration (assuming a homogeneous distribution) is only around 1% and shows the maximum intensity near the surface. The origin of the La is probably eroded material from the LaB_6 cathode. For the quantitative assessment of the composition La is ignored. However, it should be noted that the Be 1s signal is close to a La 4d signal. Boron is not detected in XPS measurements due to its low photoionization cross sections, but it is traceable by NRA.

The compositional depth profile of the W samples exposed to the deuterium plasma seeded with 0.4% Be is shown in Fig. 6(a). The arrows indicate

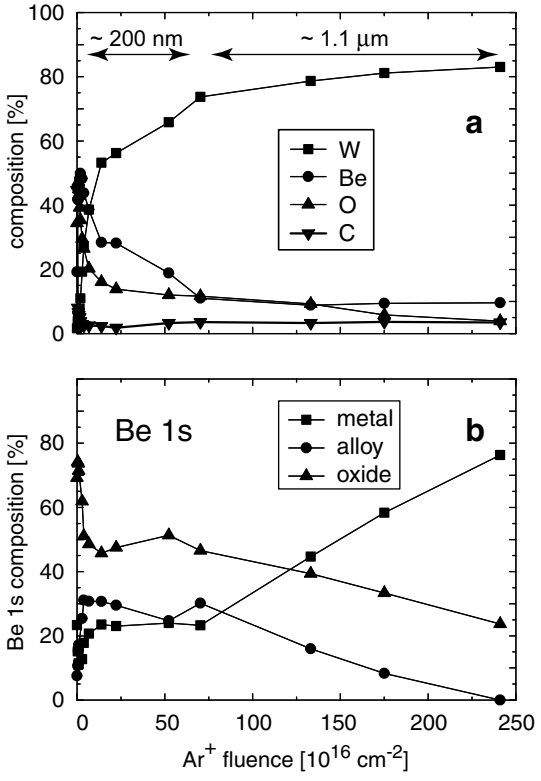

Fig. 6. Sputter depth profile of a W sample exposed to a Be-seeded deuterium plasma. Part (a) shows the elemental composition with depth. Part (b) shows the chemical composition of the Be 1s signal, determined by peak fitting.

the approximate depth, estimated by SDTRIM.SP using the composition from the XPS data. Besides the usual contamination of the first monolayers by air transport, the carbon concentration is almost constant around 3%. Oxygen is present throughout the analyzed depth, initially between 30% and 40%. At greater depths, the oxygen signal drops to 10% and below. The initially higher amounts can be related to the Be concentration. If both elements are present, BeO is the thermodynamically most stable compound. The origin of the oxygen can be either surface contamination or plasma impurities. Since the oxygen is present in greater depths, the latter explanation seems plausible. Due to the high exposure temperature, also oxygen diffusion into the bulk is possible. Up to an Ar^+ fluence of $2\times10^{16}\,cm^{-2}$ the tungsten concentration is small and reaches only around this fluence the 10% level. Therefore, the W substrate is covered by a layer consisting mainly of Be, C, and O. Above that fluence and within the first ≈200 nm, the W concentration increases in parallel to the decrease mainly of the Be component. Except in the very surface-near zone, Be and W show an opposite behavior: As much as W increases, the Be concentration decreases. Above an Ar^+ fluence of approximately $7\times10^{17}\,cm^{-2}$ W dominates the composition around 80% and above. However, during the whole analyzed depth of approximately 1.3 µm Be is present at a 10% level, whereas C and O are still at the 3–5% levels. Since also La is detected up to this depth (not shown), it seems plausible that the mixed material surface layer is produced by deposition of material from the plasma rather than by diffusive processes. However, a clear decision is not possible on the present data.

The analysis of the Be 1s BE region, shown in Fig. 6(b), allows the assessment of the Be chemistry in the deposited layer. The analyzed depth can be clearly separated in two regions, as indicated by the depth arrows in Fig. 6(a). In addition, the very surface is dominated by BeO with a concentration between 70% and 80%. This demonstrates that Be is enriched at the surface at elevated temperatures, as was shown in the case of a W layer on Be (Section 3.1). The driving force for this diffusional process can be the large enthalpy of formation of BeO and requires oxygen present at the surface (either as a plasma impurity or adsorbed by repeated air transports, as in Section 3.1). This BeO layer is reduced to below 50% above 3×10^{16} $Ar^+\,cm^{-2}$ and stays at this level up to 7×10^{17} $Ar^+\,cm^{-2}$. Within thin zone of approximately 200 nm thickness also the fractions of metallic Be and Be bound in a Be–W alloy are constant. The alloy component has around 30%, the metallic phase around 23%. The chemical shift between the metallic and alloy Be 1s signals in this depth zone is 0.6 eV. This shift is in between the shifts determined for Be_2W (0.7 eV) and $Be_{12}W$ (0.5 eV). Therefore, no clear assignment of the Be–W alloy stoichiometry is possible in this case. The large fraction of W in the surface zone, however, points towards a dominating Be_2W phase. Beyond the ≈200 nm surface zone, both alloy and oxide peaks decrease. The alloy peak is no more detectable at the end of the depth profile is fluence, at 2.4×10^{18} $Ar^+\,cm^{-2}$. At this fluence, still 24% of Be is chemically bound in BeO.

4. Conclusions

In this paper we compare three different scenarios for the interaction of Be with W and analyze the

resulting mixed material layers and compounds. The two fundamental cases are discussed first: the formation of Be–W alloy phases starting with a pure layer of one component on a bulk substrate of the respective other. The third case treats the interaction of a deuterium plasma (which is seeded with a small Be concentration) and a hot W substrate. In both cases of the layered systems, an alloy surface layer is formed. However, a strong difference in the thickness of this alloy layer is observed. In the case of a W layer on Be, the final surface layer after annealing to above 1000 K has a thickness of several μm (depending on the initially deposited amount of W). During alloying the whole available tungsten is used to form a $Be_{12}W$ alloy which is stable at the surface of the Be bulk. As a consequence, the properties of this alloy layer determine the physical properties of the material, in particular its melting point. Comparing the alloy layer with the pure metals Be and W, its melting point is approximately that of the pure Be (from the phase diagram only a marginally higher melting temperature for $Be_{12}W$ than for pure Be can be deduced). The deposited W surface layer ($T_m = 3695$ K), however, looses the property of a very high melting point completely. For the opposite system of a pure Be layer on W substrates so far only experiments with layers up to a few nm are carried out. These experiments, however, demonstrate a subtle balance between alloying (the final alloy phase above 970 K is Be_2W in this case) and sublimation of Be. In all cases of initial Be layers between 1 and 4 nm the finally formed Be_2W alloy layers have thicknesses around 1.2 nm. The excess Be is not found in greater depths, as shown in sputter depth profiles. The conclusion to this is that Be sublimates and is no longer available for alloy formation. The balance between Be sublimation and alloy formation by interdiffusion of Be and W determines the formed surface layer in this case. For the application of both Be and W in e.g. ITER, the second scenario seems more probable than the case of W layers deposited on Be. For Be layers on W, eroded Be from the main chamber needs to be transported into the baffle/divertor regions. This is the transport path for light impurities and actually a design feature. The opposite process, transport of eroded W from the baffle into the main chamber and deposition of W on the Be walls, seems very improbable due to the plasma transport properties. However, also W layers on Be might be of importance locally where W and Be surfaces are in close vicinity. Be deposited on W at elevated temperatures would lead to an alloy layer. Due to the limited thickness found in our experiments the detrimental effects of the alloy layer on W seem small, however. Finally, the exposure of W samples to a Be-seeded plasma in PISCES-B demonstrate that even under conditions of small Be concentrations in the plasma Be-containing surface layers are formed. These layers may contain even 10% of Be which is not only found in Be–W alloy phases, but also in BeO. The oxide is the Be compound with the largest enthalpy of formation and is formed together with oxygen as an impurity in the plasma. From the presently available data, measured at high substrate temperatures, the formation of thick Be-containing layers cannot be excluded even for very low Be plasma concentrations. This could be due to Be diffusion caused by the constant influx of Be to the surface. More experiments of this kind are necessary to asses the temperature influence on the composition of the formed Be-containing mixed materials under plasma exposure.

References

[1] R.R. Parker, Nucl. Fusion 40 (2000) 473.
[2] T.B. Massalski, H. Okamoto, P.R. Subramanian, L. Kacprzak, Binary Alloy Phase Diagrams, 2nd Ed., ASM International, Materials Park, Ohio, 1996, Version 1.0.
[3] M.P. Seah, I.S. Gilmore, G. Beamson, Surf. Interface Anal. 26 (1998) 642.
[4] MultiPak, Ver. 7.0.1, Physical Electronics, 2004.
[5] N.P. Barradas, C. Jeynes, R.P. Webb, Appl. Phys. Lett. 71 (1997) 291.
[6] M. Mayer, SIMNRA User's Guide, Report IPP 9/113, Max-Planck-Institut für Plasmaphysik, Garching, Germany, 1997. <http://www.rzg.mpg.de/~mam/, mailto:matej.mayer@ipp.mpg.de>.
[7] R.G. Thomas et al., Phys. Rev. 75 (1949) 1612.
[8] A. Wiltner, Ch. Linsmeier, J. Nucl. Mater. 337–339 (2005) 951.
[9] A. Wiltner, Ch. Linsmeier, New J. Phys. 8 (2006) 181.
[10] E. Taglauer, W. Heiland, in: P. Varga, G. Betz, F.P. Viehböck (Eds.), Proceedings of the International Symposium on Sputtering, Inst. Allg. Phys. TU Wien, 1980, p. 423.
[11] W. Eckstein, Computer Simulation of Ion–Solid Interactions, Springer Series in Materials Science, vol. 10, Springer, Berlin, 1991.
[12] J.F. Moulder, W.F. Stickle, P.E. Sobol, K.E. Bomben, in: J. Chastain (Ed.), Handbook of X-ray Photoelectron Spectroscopy, Perkin–Elmer Corp. Eden Prairie, 1992.
[13] A. Wiltner, Ch. Linsmeier, Phys. Status Solidi A 201 (2004) 881.
[14] R. Doerner, M. Baldwin, K. Schmid, Phys. Scr. T111 (2004) 71.
[15] A.S. Kukushkin, H.D. Pacher, D.P. Coster, et al., J. Nucl. Mater. 337–330 (2005) 50.